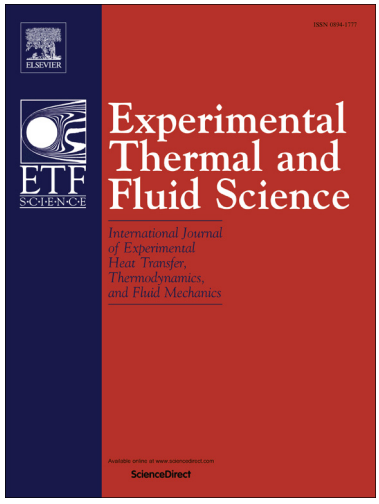

Analysis of fluid hammer occurrence with phase change and column separation due to fast valve opening by means of flow visualization

Marcos Lema, Fernando López Peña, Jean-Marie Buchlin, Patrick Rambaud, Johan Steelant

PII: S0894-1777(16)30180-7
DOI: http://dx.doi.org/10.1016/j.expthermflusci.2016.07.008
Reference: ETF 8822

To appear in: *Experimental Thermal and Fluid Science*

Received Date: 8 February 2016
Revised Date: 30 June 2016
Accepted Date: 6 July 2016

Please cite this article as: M. Lema, F.L. Peña, J-M. Buchlin, P. Rambaud, J. Steelant, Analysis of fluid hammer occurrence with phase change and column separation due to fast valve opening by means of flow visualization, *Experimental Thermal and Fluid Science* (2016), doi: http://dx.doi.org/10.1016/j.expthermflusci.2016.07.008

Analysis of fluid hammer occurrence with phase change and column separation due to fast valve opening by means of flow visualization

Marcos Lema

Universidade da Coruña, Maestranza s/n, 15001 A Coruña, Spain

Fernando López Peña

Universidade da Coruña, Maestranza s/n, 15001 A Coruña, Spain

Jean-Marie Buchlin

von Karman Institute for Fluid Dynamics, Chaussée de Waterloo, 72, B-1640 Rhode-Saint-Genése, Belgium

Patrick Rambaud

von Karman Institute for Fluid Dynamics, Chaussée de Waterloo, 72, B-1640 Rhode-Saint-Genése, Belgium

Johan Steelant

European Space Agency, Keplerlaan 1, P.O. Box 299, 2200 AG Noordwijk,The Netherlands

Abstract

This paper presents an experimental investigation on the fluid hammer phenomenon generated when filling a pipe line under vacuum conditions with a closed end. This physical configuration, although it can be found in many piping configurations, it is of special interest in propulsion systems of satellites during priming operation. The fluid hammer taking place here not only leads to high pressure peaks in the fluid but also to low pressures, which can cause cavitation, gas desorption and liquid column separation.

The study is carried out on a facility allowing flow visualization, which is achieved by replacing the pipe closed end by a quartz cylinder drilled with the

*Corresponding author
Email address: marcos.lema@udc.gal (Marcos Lema)

same tube inner diameter. In this way, the flow can be recorded with high speed imaging at this location. The visualizations confirm that the pressure evolution is accompanied by a complex multiphase flow pattern. First of all, a foamy mixture of non-condensable gas, vapor and liquid droplets precedes the liquid front arrival at the bottom end. During the fluid hammer compression wave, the vapor condensates and the non-condensable gas gets compressed. Afterwards, the arrival of an expansion wave induces the movement of the liquid column backwards, with the corresponding pressure drop that generates a gaseous bubble referred to as column separation. Finally, the collapse of this bubble is at the origin of the next pressure rise.

Keywords: `f`luid hammer, flow visualization, gas absorption/desorption, cavitation, column separation, priming

1. Introduction

The presence of a closed end in a piping system generates a fluid hammer when the flow is suddenly brought to rest. This scenario is particularly hazardous when a liquid fills a pipe line under vacuum conditions by opening a fast valve. This physical configuration induces a high acceleration of the flow before going to rest at a closed end, inducing the subsequent fluid hammer pressure rise. This is the case of propulsion systems used in satellites during priming operation, where the propellant lines initially kept under vacuum conditions are filled with liquid propellant by opening a pyrotechnic valve.

Fluid hammer during priming not only leads to high pressure peaks in the fluid but also to low pressures, which can cause cavitation. In particular, the propellant is pressurized in the tanks with a non-condensable gas (NCG) that dissolves in the liquid during storage. When the valve opens, the new pressure conditions are below the saturation pressure, inducing the desorption of the NCG, and if the pressure in the line is also below the vapor pressure, in addition the liquid undergoes cavitation.

Therefore, two types of cavitation can be originated in liquid filled pipes,

as summarized in the review by Bergant et al. [1]. Gaseous cavitation occurs when the pressure falls below the saturation pressure of the gas that may be dissolved in the liquid. Vaporous cavitation occurs when the pressure drops below the liquid vapor pressure and vapor cavities develop in the liquid. In vaporous cavitation two types are distinguished, based on the magnitude of the void fraction of the vapor, α_v, which expresses the fraction of the vapor volume, V_v, in a given volume of fluid, V (vapor + liquid).

$$\alpha_v = \frac{V_v}{V} \tag{1}$$

For low values of α_v ($\alpha_v \approx 0$), tiny bubbles are dispersed throughout the liquid. It is referred to as dispersed cavitation (or flashing). This type of cavitation occurs over an extended length of the pipe. When the vapor cavities coalesce, they create a single local bubble occupying a large part of the pipe cross-section ($\alpha_v \approx 1$). In this case, it is referred to as column separation. The collapse of the cavities during a fluid hammer event may cause short duration pressure peaks exceeding those computed with the Joukowski equation [2, 3], producing secondary pressure peaks in the flow.

Based on the volumetric ratio of gas and liquid phase, Weisman [4] summarized the regimes that may occur in an air/water mixture in a vertical pipe. Brennen [5] adapted this classification to describe the flow pattern in a vertical pipe shown in figure 1. The regimes represented here go from bubbly flow, where gas bubbles appear in the bulk liquid flow, to disperse flow (not to be confused with dispersed cavitation), where liquid drops travel within the gas flow. In a cavitation regime, slug and churn flow are the result of vapor bubbles coalescencing, while the annular flow is typically observed during column separation.

Flows undergoing column separation can be classified according to the Cavitation Severity Index, S, which was proposed by Martin [6]. This index is expressed as a function of the wave speed in the fluid, c, the characteristic pipe lenght, L, and the duration of the column separation, t_c. In cases with

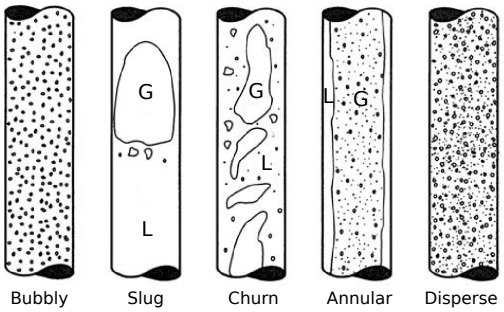

Figure 1: Flow regimes representation for two-phase flow in a vertical pipe. From [4] and adapted by [5]

cavitation, S cannot be lower than one for any amount of cavitation.

$$S = \frac{t_c}{2L/c} \tag{2}$$

The presence of a NCG is addressed in gaseous cavitation. One of the main features of liquids is their capability of absorbing a given amount of gas to which they come into contact through a free surface. According to Henry' s law [7], at constant temperature, the amount of gas dissolved in a liquid volume is directly proportional to the partial pressure of the gas in equilibrium with the liquid. Gas release is a diffusive process that can be very fast. On the other hand, the absorption process from the gaseous state to the dissolved liquid state has to overcome the surface tension effect and therefore will always take longer than the desorption/release process. The presence of gas bubbles in the liquid can drastically reduce the wave velocity, as described in the classic textbook by Wylie and Streeter [8].

The objective of this paper is to give an insight towards the understanding of the multiphase behavior of the flow during fluid hammer occurrence through flow visualizations. Bunker and Lee [9] have already used high speed imaging to visualize the hydrazine compression during priming. In this paper, the fluid hammer mechanism is characterized with snapshots extracted from the flow visualizations in a transparent pipe segment. To our knowledge, this type of analysis is done for the first time with images of a liquid front brought to rest

at a closed end of a piping line.

For this purpose, an experimental facility is designed and built, where a pressurized liquid at $2\,MPa$ is discharged by fast opening a valve in a pipe line vacuum pumped at $1\,kPa$ or $10\,kPa$. The pipe closed end consists of a quartz drilled cylinder, allowing optical access for recording the flow with high speed camera. The facility is run with three inert fluids, such as water, ethanol and acetaldehyde, and where the liquid saturation conditions with the pressuring gas can be controlled. The ability to work with saturated and fully deaerated liquids is a novel characteristic of this facility, which is not found in past studies [10, 11, 12, 13].

2. Experimental facility

The experimental facility used in the present study is basically designed to reproduce the priming procedure in satellites [14, 15, 16, 17, 18, 19, 10, 11], including all the elements of a satellite propulsion system involved in the fluid hammer occurrence, i.e. a pressurized liquid tank, a fast opening valve (FOV), consisting of a ball valve with a pneumatic actuator, and a $2\,m$ pipe line referred to as "test element". The test element is made of the same titanium tube used for aerospace applications (alloy T3AL2.5V, specification AMS4943H), with $0.25\,in$ $(6.35\,mm)$ of inner diameter and $0.016\,in$ $(0.4\,mm)$ thickness.

The facility layout, presented in figure 2, also includes a vacuum system to set the test conditions in the propellant line. The test procedure starts by filling the tank with the working liquid to be later pressurized by means of compressed NCG. The facility is ready for a test when the test element is vacuum pumped until a certain pressure, the FOV closed, and the pipe segment between the tank and the FOV filled with the pressurized working liquid. The accelerating liquid flow is generated by opening the FOV in less than $40\,ms$. A measurement module is attached at the bottom end of the test element, highlighted in figure 2, which is the impact location where the fluid hammer is induced and the most significant multiphase phenomena occur. Two measurements modules have

been constructed, an instrumented module with unsteady pressure transducers, and a transparent module to allow liquid flow visualizations. A more detailed description of the facility and the pressure measurements can be found in [20, 21] by the same authors, while the transparent module will be described in section 3.

A parameter that plays an important role in the fluid hammer occurrence is the saturation level of the working fluid with the NCG. In normal conditions, the driving pressure gas gets dissolved in the liquid through a diffusive process, and the saturation level is defined by the pressure applied to the NCG during storage. For this reason, on the test vessel an elastic membrane is mounted to avoid the absorption of the NCG during the liquid pressurization for tests with fully deaerated liquids. The deaerated condition is set by applying a degasification process to the test liquid, and it is achieved by keeping the liquid under reduced pressure, often referred to as vacuum degasification. The deaeration vessel used for this purpose, shown in figure 2, also features a membrane to allow the transfer of the deaerated liquid to the test vessel avoiding the contact of the driving pressure gas with the liquid. In case the liquid needs to be under saturated conditions, NCG is first blown in the test vessel to be later filled with deaerated liquid. In that way, the contact of the two phases is ensured during tank pressurization. A more detailed description of the facility and the test procedure can be found elsewhere by the same authors [21].

3. Flow visualization

The transparent module used in this study is designed for flow visualizations with high speed imaging techniques at the impact location, i.e. at the bottom end of the test element as figure 2 shows. This transparent module is made out of Quartz, with the same internal diameter as the test element (see figure 3). Due to the difficulties in manufacturing quartz crystal with the required tolerance, the design of this module has been simplified: a solid quartz cylinder was drilled. This design makes it necessary to use a metallic bottom end plate,

on which the liquid front will impact. The test element connector is screwed on a first plate and the transparent module is mounted tight between the two disks by means of six bolts (see figure 4). An evacuation plug was added to the bottom plate to empty the test liquid after each test.

In order to avoid optical aberration due to the external curved surface of the transparent module, the whole module is submerged in a square water tank with methacrylate walls. In this way, since the water, the quartz and the methacrylate have nearly the same refraction index, the flow visualization can be carried out without distortion on the flat surfaces of the water tank. The resulting assembly is shown in figure 5.

The videos are recorded with a Phantom high-speed camera from Vision Research, using a sampling rate of 7005 images per second with a resolution of 64×464 pixels. Exposure time varies from $10\,\mu s$ and $20\,\mu s$ depending on the module orientation and illumination conditions.

4. Flow description and analysis

The results of flow visualization will be now presented based on the most representative snapshots recorded at the impact location. The snapshots presented hereafter are extracted from the time lapse between the FOV opening and the second pressure peak, which show the most interesting features taking place during fluid hammer occurrence. The images are presented chronologically from left to right and top to bottom, and they are accompanied by the pressure evolution obtained with an instrumented measurement module to help on the understanding of the whole fluid hammer process. The measurements with the instrumented module can be found in the article by the same authors [21].

4.1. Results with deaerated liquids

In figure 6, the results obtained with water are presented when the vacuum level in the pipe line is $P_p = 1\,kPa$. In the first snapshot, the FOV is still closed

and the test element is vacuum pumped. The module appears completely empty, with the tube walls clearly identified due to different refraction indexes of the gas phase and quartz. Surprisingly, a few instants after the valve starts to open, dispersed droplets arrive to the bottom, followed by visible liquid pockets in snapshot 2. It is believed that this behavior is a consequence of the flashing flow during valve opening. Unfortunately, the liquid vapor that may be generated during the opening process cannot be distinguished in the images. On the other hand, the foamy mixture of liquid, vapor and NCG preceding the liquid front arrival appears dark colored in the images, as it can be clearly observed in snapshot 3. Here, the gas in the mixture comes from the residual NCG initially left in the line. Finally, the liquid front arrives and the induced pressure rise starts to condense the vapor phase and compresses the NCG dissolved in the liquid, as can be observed in snapshot 4.

When the pressure reaches its maximum, and for the duration of the pressure peak, the module appears full of liquid, as in snapshot 5. In this case, the images appear completely white due to the matching refraction indexes of quartz and water. According to this image, one might think that the NCG has been completely dissolved in the liquid, but taking into account the duration of the pressure peak, the hypothesis of absorption must be rejected. On the other hand, when the reflected expansion wave from the tank approaches the bottom end, the pressure decreases almost instantaneously at this location and the NCG starts to expand, inducing a bubbly flow. This can be observed in snapshot 6, where tiny gas bubbles grow within the liquid. The pressure drop is accompanied by the liquid column acceleration towards the tank, inducing the liquid column separation at the bottom end. The column separation leaves behind a foamy mixture of liquid, vapor and NCG (referred to as multiphase bubble), identified in snapshot 7. As the column continues moving towards the tank, the volume occupied by the multiphase mixture grows, inducing the coalescence of the gaseous bubbles, as can be already distinguished in snapshot 8. Snapshot 9 shows the instant where the liquid column has reached its maximum displacement upwards, and all the gas bubbles have nearly merged in a single

bubble with a liquid film wetting the inner pipe wall. This regime can be defined by [4] and [5] as annular flow.

From now on, the liquid column starts to move back towards the bottom end and the front can be seen again coming from the top of snapshot 10. As the front moves downwards, the multiphase bubble is compressed with a minor presence of foam pockets as observed in snapshot 11. Finally, in snapshot 12 the liquid front reaches again the bottom end and a new pressure rise takes place, which condenses once more the liquid vapor and compresses the NCG. This situation is analogous to the one represented in snapshot 5. The column separation and the later impact at the bottom end defines the time delay between peaks.

The same snapshot representation is also used for the other test liquids used in this study. The flow visualization with deaerated ethanol is presented in figure 7 and with deaerated acetaldehyde in figure 8, where one can distinguish the same flow sequence described previously with water: liquid pockets arrival, foamy mixture preceding the liquid front, NCG compression, front impact, liquid column moving upstream, foamy mixture, column separation, ending with a new impact of the liquid front against the bottom end. The main difference observed comes from the nature of the multiphase bubble during column separation, mainly in snapshots 8 and 9 from figure 7. Now, the initial foamy mixture does not become the (almost) unique (gaseous) bubble found with water. Instead, the whole volume left during column separation is filled with a bubbly flow. The same behavior is observed in the flow visualization made with acetaldehyde in figure 8. Once more, snapshots 8 and 9 show the volume filled with a bubbly flow. Acetaldehyde and ethanol share nearly the same surface tension ($\sigma = 21.2\,mN/m$ and $\sigma = 22.27\,mN/m$ for acetaldehyde and ethanol, respectively, and $\sigma = 72.85\,mN/m$ for water) that may explain the similar behavior observed during column separation. Indeed, the Hinze's scale proposed by [22], and successfully applied by many authors as in [23] and [24], allows to compute the maximum bubble diameter as:

$$d_{max} = 0.725 \left(\frac{\sigma}{\rho_l}\right)^{3/5} \epsilon^{-2/5} \tag{3}$$

where ϵ is the turbulent kinetic energy dissipation rate. According to equation 3, the lower the surface tension of the liquid, the easier the transition to dispersed bubble regime. This would explain the behavior observed in the multiphase bubble with deaerated ethanol and deaerated acetaldehyde, which is not found with water.

When the initial pressure in the test line is increased up to $P_p = 10\,kPa$, the amount of residual gas increases accordingly. This fact causes two main differences in the flow compared to the results with $P_p = 1\,kPa$. First of all, during the highest pressure rise, bubbles of NCG are always noticeable at the bottom end, as a consequence of both lower pressure rise and higher amount of NCG. This fact can be observed in figure 9, which shows the snapshots at the highest pressure rise for the three liquids.

The other difference is related to the multiphase bubble growing during column separation. When $P_p = 10\,kPa$, there is more NCG to fill the volume left behind the liquid column, with the development of the annular flow, even for ethanol and acetaldehyde despite their low surface tension. Figure 10 shows the instant where the liquid column has reached its maximum displacement upwards and the bubble occupies the largest volume in the tube.

4.2. Results with saturated liquids

Liquids under saturation conditions are drastically affected by the dissolved gas phase during fluid hammer occurrence, mainly when the liquid experiences a high desorption rate. The authors concluded in [21] that in liquids with a low gas desorption rate, as water, the dissolved gas phase hardly affects the fluid hammer phenomenon. For this reason, water visualizations shown in figure 11 offers nearly the same flow sequence as represented in figure 6.

On the other hand, saturated ethanol and acetaldehyde experience an intense gas desorption rate during fluid hammer occurrence, damping the pressure level and shortening the attenuation process. As a consequence of this behavior, the

flow patterns observed in figures 12 and 13 change completely, mainly because column separation does not take place. The massive arrival of evolved NCG not only decreases the initial pressure rise, but also adds compressibility to the fluid, allowing the movement of the liquid column towards the tank by expanding the volume of gas bubble mixed within the liquid. Furthermore, the foamy mixture that now precedes the acetaldehyde front arrival, which was not observed when $P_p = 1\,kPa$, indicates that gas desorption already starts during FOV opening.

Figures 12 and 13 illustrate this description, where the NCG volumes compress and expand according to the traveling pressure waves, but the liquid column is never detached from the bottom end.

The column separation and the later impact at the bottom end defines the time delay between peaks. When the column separation does not take place, the time delay between peaks is defined by the time needed by the pressure wave to travel back and forth to the tank and bottom end. In this process, the pressure peaks are progressively attenuated by viscous dissipation.

5. Conclusions

This paper presents flow visualizations recorded during fluid hammer occurrence by means of high speed imaging. This is achieved by replacing the closed end of the pipe line by a transparent quartz module. The aim is to analyze the multiphase nature of the flow during fluid hammer occurrence. To our knowledge, this is the first time that the fluid hammer phenomenon is characterized with flow visualizations.

The fluid hammer is generated in a dedicated facility, run with three inert fluids, and two vacuum pressure levels in the pipe line. The presentation of the results with a sequence of snapshots allows distinguishing the foamy mixture preceding the liquid front and the NCG compression when the front impacts at the bottom end, the subsequent column separation with the creation of a multiphase bubble, ending with a new impact of the separated liquid column against the bottom end. The nature of the multiphase bubble is different for the

three liquids when $P_p = 1\,kPa$: water leaves an annular flow behind the column, while ethanol and acetaldehyde induce a bubbly flow. The lower surface tension of these two liquids would explain this behavior.

The higher presence of residual gas when $P_p = 10\,kPa$ is noticeable in the visualizations, both during the pressure peaks with visible NCG pockets, and during column separation with the development of an annular flow with all the test liquids. Finally, liquid column separation does not take place when ethanol and acetaldehyde are tested under saturated conditions, since gas desorption is very effective in these liquids and the growing amount of evolved NCG in the line drastically increases the fluid compressibility.

Acknowledgements

The present research activity was initiated and promoted by the European Space Research and Technology Centre of the European Space Agency (ESTEC/ESA) through the GSTP activity AO/1-6210/09/NL/CP.

References

[1] A. Bergant, A. R. Simpson, A. S. Tijsseling, Water hammer with column separation: a historical review, Journal of Fluids and Structures 22 (2006) 135–171.

[2] N. Joukowsky, On the hydraulic hammer in water supply pipes (french translation), in: Annales des Ponts et Chausses; Mémoires et Documents, Ministre Des Travaux Publics, 1907.

[3] L. Allievi, General theory of the variable motion of water in pressure conduits (french translation), in: Revue de Mécanique, Paris, 1904.

[4] J. Weisman, Two-phase flow patterns, Ann Arbor Science, 1983, Ch. 15 in Handbook of Fluids in Motion, pp. 409–425.

[5] C. E. Brennen, Fundamentals of multiphase flow, Cambridge University Press, 2005.

[6] C. S. Martin, Experimental investigation of column separation with rapid closure of downstream valve, in: 4th International Conference on Pressure Surges, 1983.

[7] C. E. Brennen, Cavitation and bubble dynamics, Oxford University Press, 1995.

[8] E. B. Wylie, V. L. Streeter, Fluid transients, McGraw-Hill Inc., 1978.

[9] R. L. Bunker, D. L. Baker, J. H. S. Lee, Explosive decomposition of hydrazine by rapid compression of a gas volume, Tech. rep., Johnson Space Center, White Sands Test Facility (1990).

[10] I. Gibek, Y. Maisonneuve, Waterhammer tests with real propellants, in: proceedings of 41st AIAA/ASME/SAE/ASEE Joint Propulsion Conference & Exhibit, Tucson (AZ), USA, 10-13 July, no. 2005–4081, 2005.

[11] R. Lecourt, J. Steelant, Experimental investigation of water hammer in simplified feed lines of satellite propulsion systems, Journal of Propulsion and Power 23(6) (2007) 1214–1224.

[12] P. Porca, M. Lema, P. Rambaud, J. Steelant, Experimental and numerical multiphase-front fluid hammer, Journal of Propulsion and Power 30 (2) (2014) 368–376.

[13] J. Pinho, M. Lema, P. Rambaud, J. Steelant, Multiphase investigation of water hammer phenomenon using the full cavitation model, Journal of Propulsion and Power 30 (1) (2014) 105–113.

[14] K. L. Yaggy, Analysis of propellant flow into evacuated and pressurized lines, in: 20th AIAA/SAE/ASME Joint Propulsion Conference and Exhibit, 1984.

[15] R. P. Prickett, E. Mayer, J. Hermal, Water hammer in a spacecraft propellant feed system, Journal of Propulsion and Power 8 (3) (1992) 592–597.

[16] T. Y. Lin, D. Baker, Analysis and testing of propellant feed system priming process, Journal of Propulsion and Power 11 (3) (1995) 505–512.

[17] J. Molinsky, Water hammer test of the seastar hydrazine propulsion system, in: 33rd AlAA/ASME/SAE/ASEE Joint Propulsion Conference & Exhibit, 1997.

[18] C. Y. Joh, K. D. Park, Pressure surge analysis and reduction in the kompsat propellant feed system, in: Proceedings KORUS 2000. The 4th Korea-Russia International Symposium on Science and Technology, 2000.

[19] M. J. Morgan, Pressure transient characterization test for star-2 propulsion system fuel manifold, in: 40th AIAA/ASME/SAE/ASEE Joint Propulsion Conference and Exhibit, 2004.

[20] M. Lema, J. Steelant, F. López Peña, P. Rambaud, J.-M. Buchlin, Experiments on fluid hammer involving cavitation and pressurant gas desorption for aerospace applications, in: 50th AIAA/ASME/SAE/ASEE Joint Propulsion Conference. Cleveland, USA, 2014.

[21] M. Lema, F. López Peña, P. Rambaud, J.-M. Buchlin, J. Steelant, Fluid hammer with gas desorption in a liquid filling tube: experiments with three different liquids, Experiments in Fluids 56 (9) (2015) 180 – 192.

[22] J. O. Hinze, Fundamentals of the hydrodynamic mechanism of splitting in dispersion processes, A.I.Ch.E. Journal 1 (1) (1955) 289–295.

[23] M. Sevik, S. H. Park, The splitting of drops and bubbles by turbulent fluid flow, Journal of Fluids Engineering 95 (1973) 53–60.

[24] N. Brauner, The prediction of dispersed flows boundaries in liquid-liquid and gas-liquid systems, International Journal of Multiphase Flow 27 (2001) 885–910.

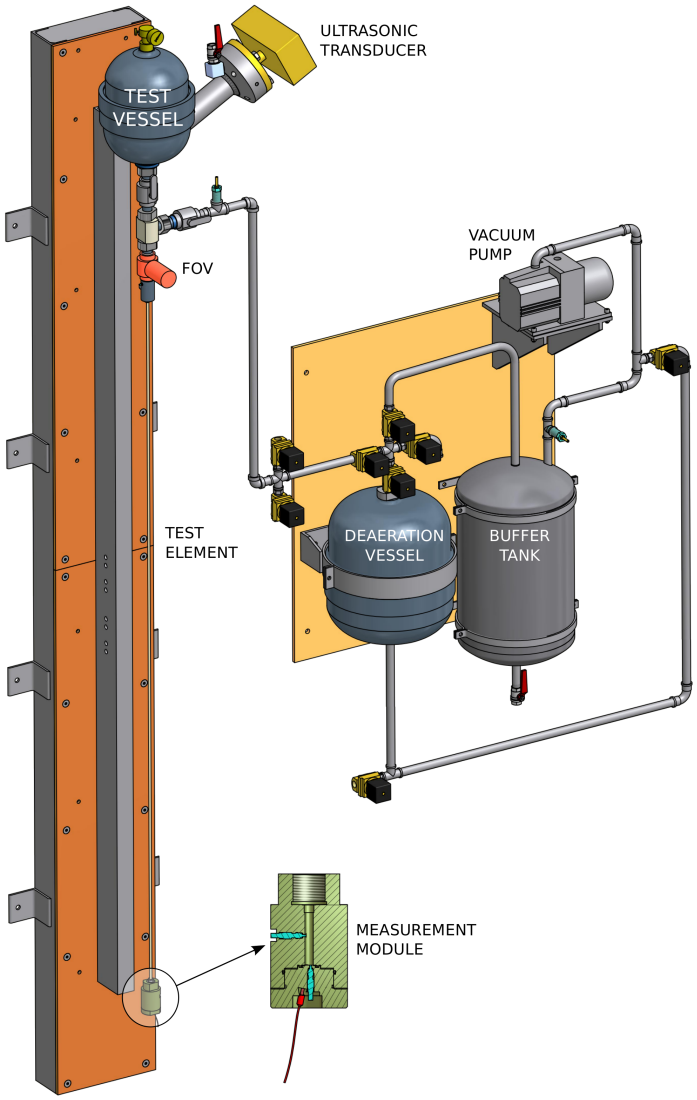

Figure 2: Experimental facility layout

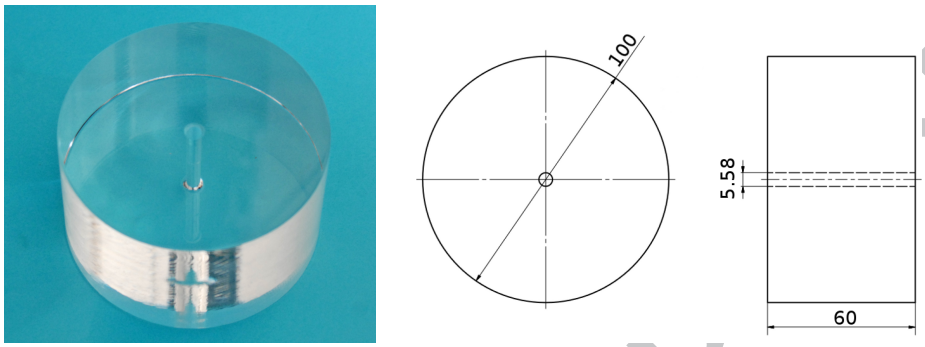

Figure 3: Transparent module built in quartz (all dimensions in mm)

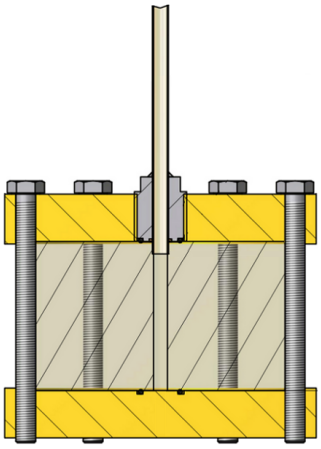

Figure 4: Transparent module assembly

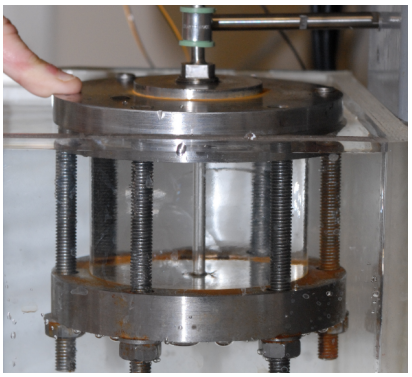

Figure 5: Module installation to avoid optical distortion

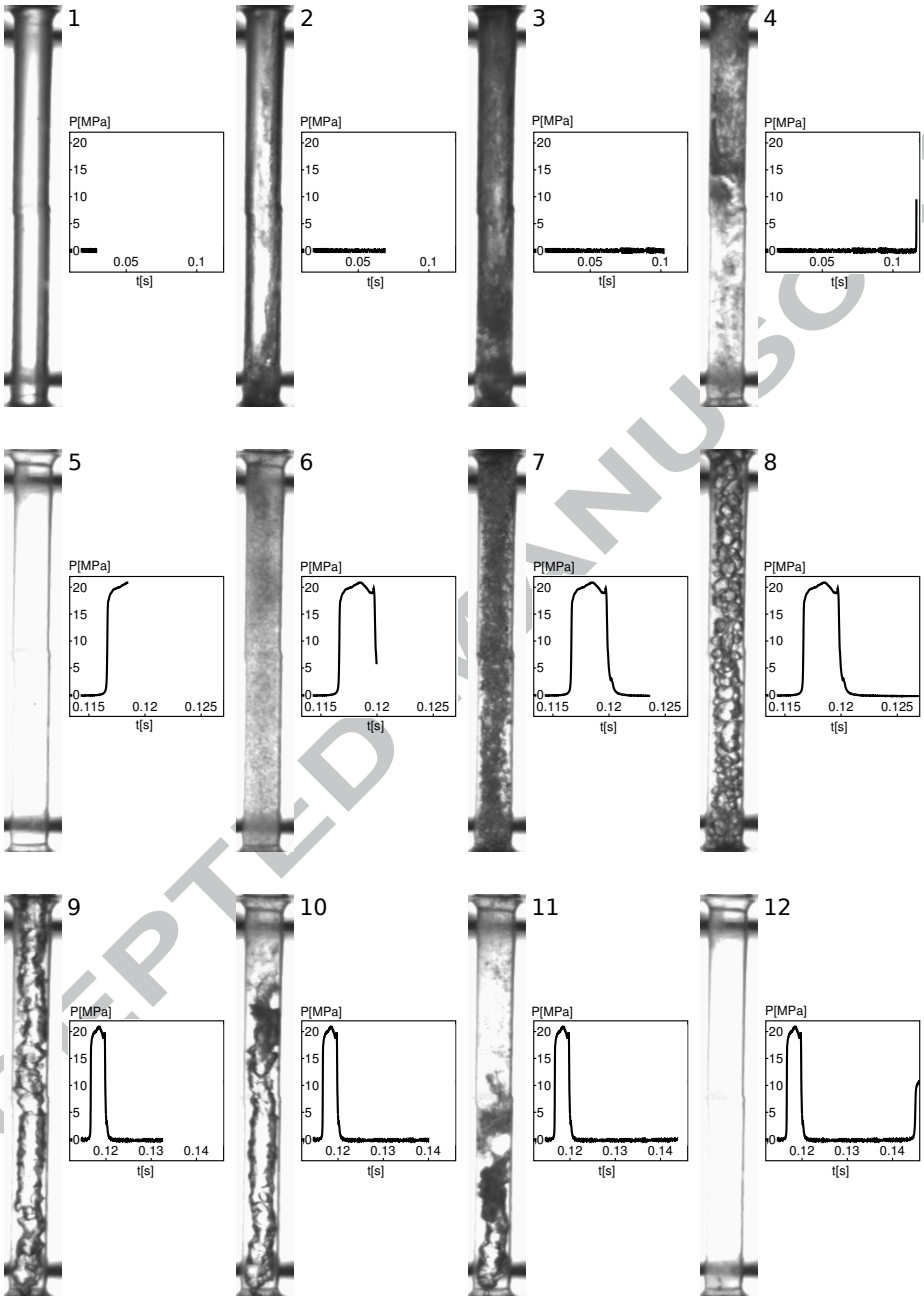

Figure 6: Liquid front visualization obtained with deaerated water in the straight configuration. Test conditions: $P_T = 2\,MPa$ and $P_p = 1\,kPa$

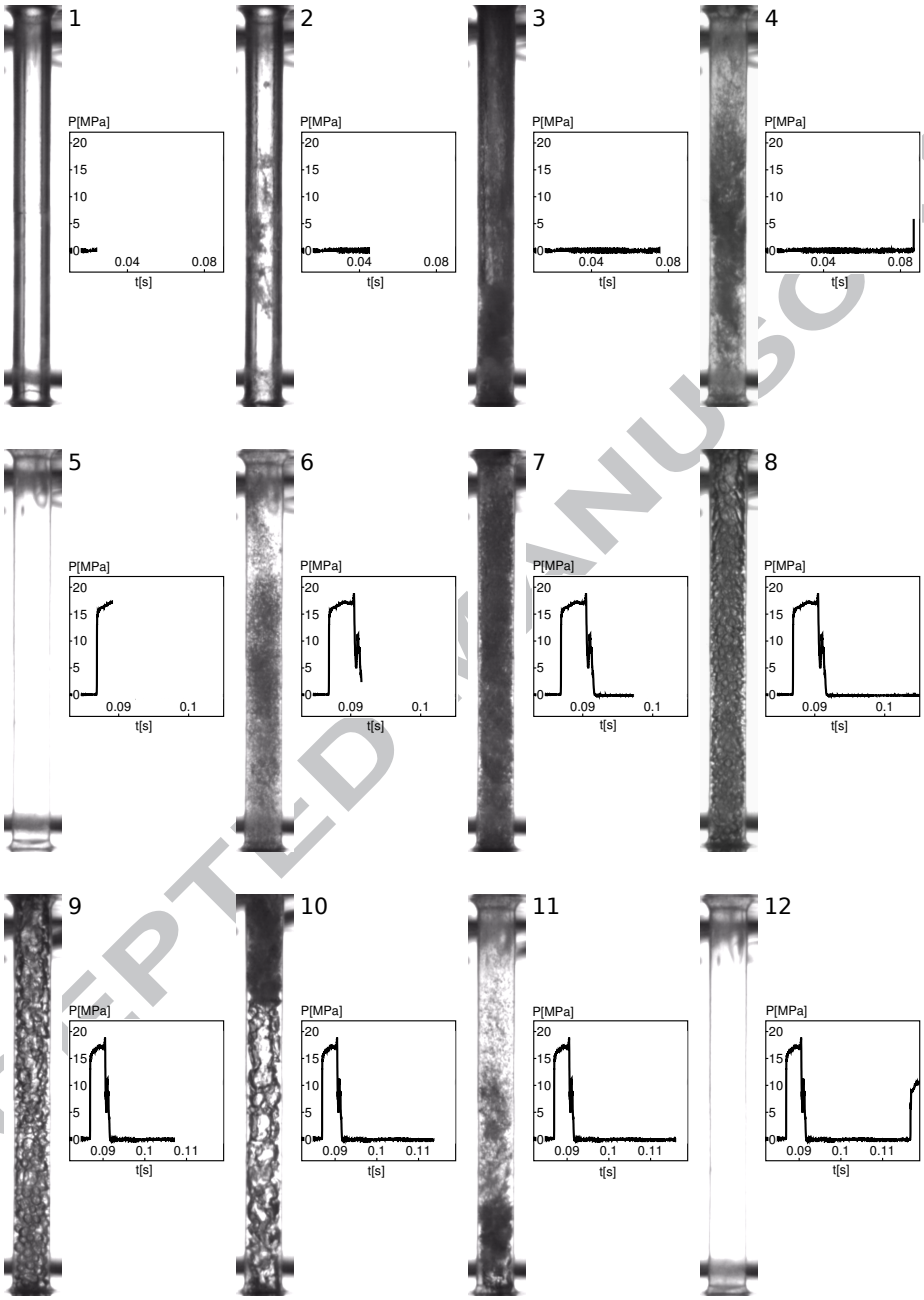

Figure 7: Liquid front visualization obtained with deaerated ethanol in the straight configuration. Test conditions: $P_T = 2\,MPa$ and $P_p = 1\,kPa$

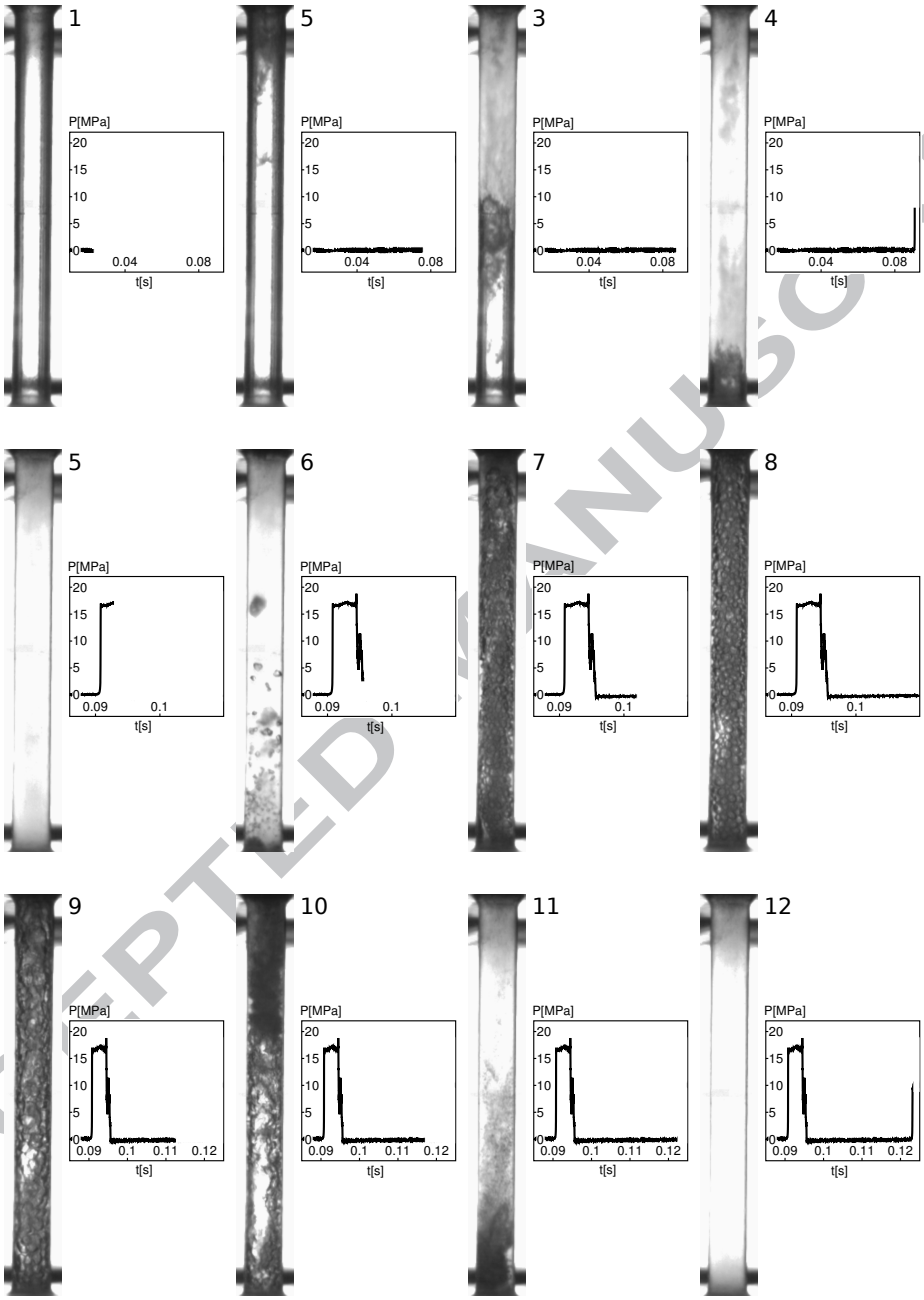

Figure 8: Liquid front visualization obtained with deaerated acetaldehyde in the straight configuration. Test conditions: $P_T = 2\,MPa$ and $P_p = 1\,kPa$

Figure 9: Snapshots recorded at the maximum pressure rise: water (left), ethanol (center), acetaldehyde (right). Test conditions: deaerated liquids, $P_T = 2\,MPa$ and $P_p = 10\,kPa$

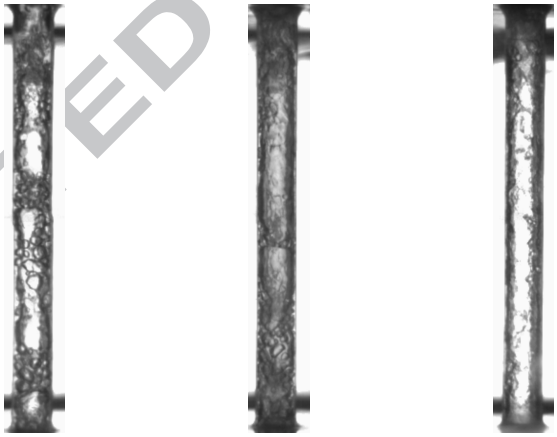

Figure 10: Snapshots of the multiphase bubble: water (left), ethanol (center), acetaldehyde (right). Test conditions: deaerated liquids, $P_T = 2\,MPa$ and $P_p = 10\,kPa$

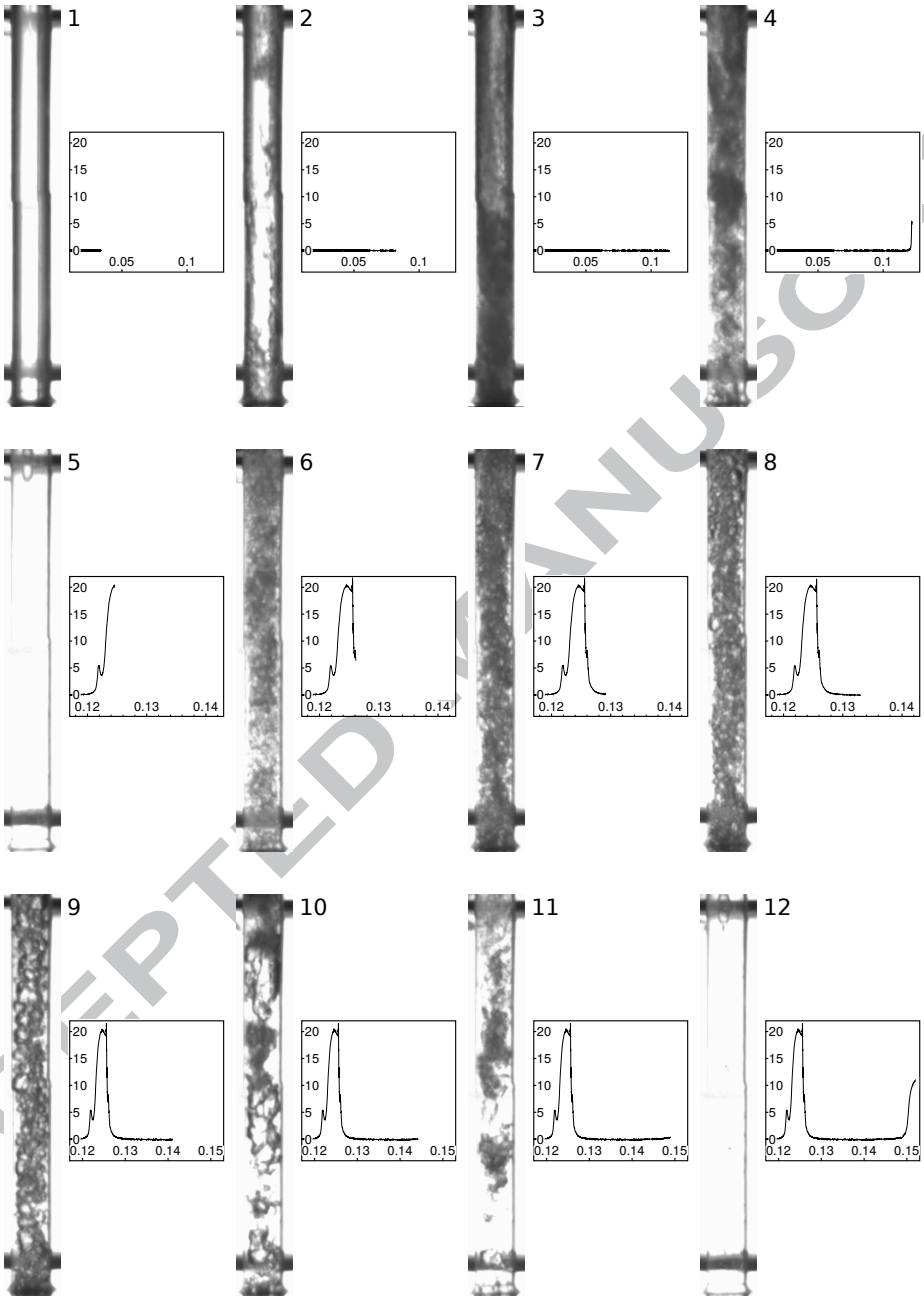

Figure 11: Liquid front visualization obtained with saturated water in the straight configuration. Test conditions: $P_T = 2\,MPa$ and $P_p = 1\,kPa$

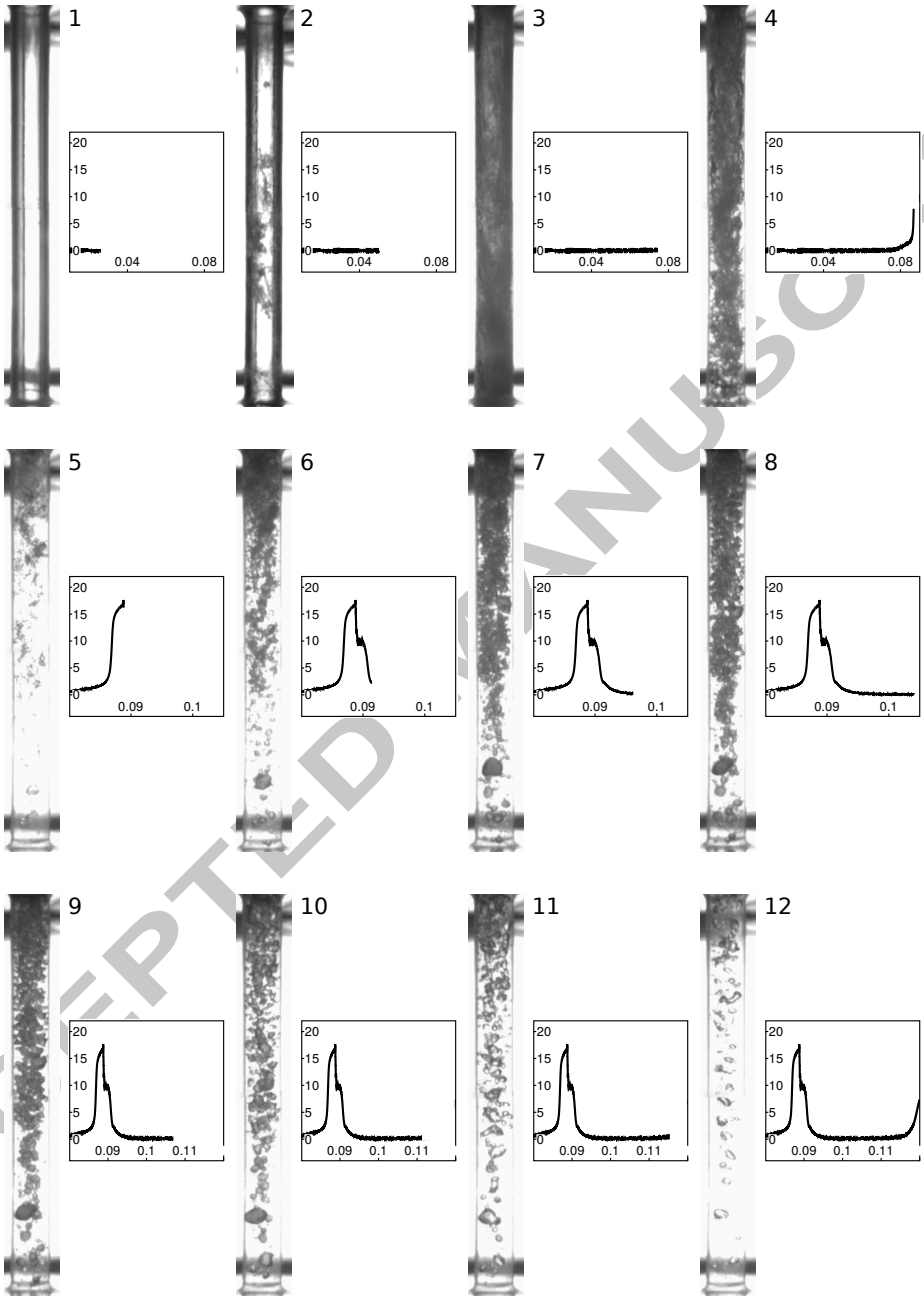

Figure 12: Liquid front visualization obtained with saturated ethanol in the straight configuration. Test conditions: $P_T = 2\,MPa$ and $P_p = 1\,kPa$

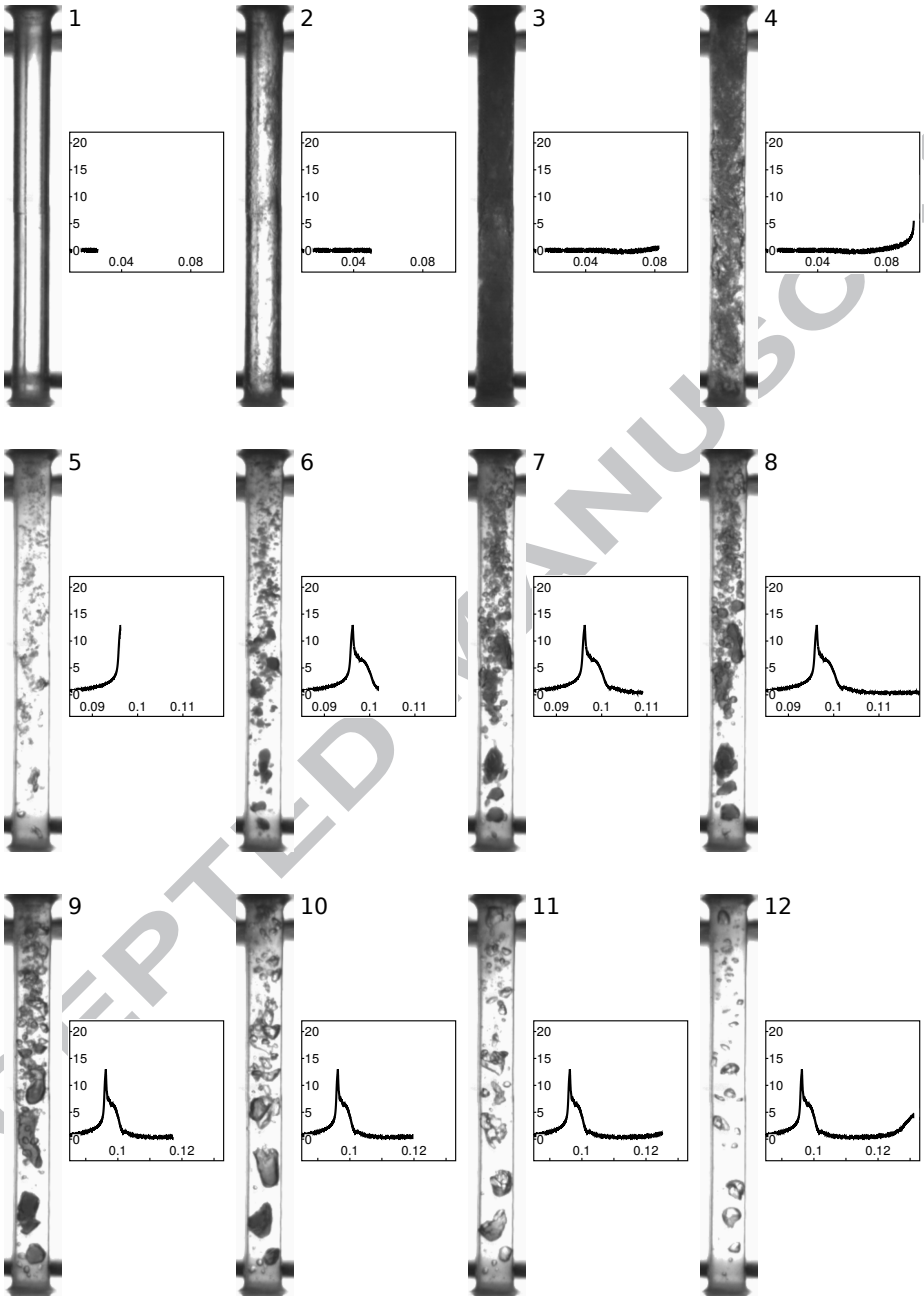

Figure 13: Liquid front visualization obtained with saturated acetaldehyde in the straight configuration. Test conditions: $P_T = 2\,MPa$ and $P_p = 1\,kPa$

- Flow visualizations recorded during fluid hammer occurrence with high speed imaging.
- Dedicated test facility run with liquids under saturated and deaerated conditions.
- Fluid hammer induces column separation of the liquid column
- Gas desorption greatly affects the fluid hammer phenomenon